ACS OMEGA

http://pubs.acs.org/journal/acsodf

Article

Advancement of Microwave-Assisted Biosynthesis for Preparing Au Nanoparticles Using *Ganoderma lucidum* Extract and Evaluation of Their Catalytic Reduction of 4-Nitrophenol

Vinh Phu Nguyen, Hieu Le Trung, Thu Huong Nguyen, DongQuy Hoang,* and Thai Hoa Tran*

Cite This: *ACS Omega* 2021, 6, 32198–32207

Read Online

ACCESS | Metrics & More | Article Recommendations

ABSTRACT: This study describes the biosynthesis of gold nanoparticles (AuNPs) using the extract of *Ganoderma lucidum* in the buffer zone of Bach Ma National Park, Vietnam, as a reducing and protecting agent using microwave-assisted synthesis. The as-synthesized AuNPs were characterized using transmission electron microscopy, scanning electron microscopy, X-ray diffraction, energy-dispersive X-ray spectroscopy, and Fourier transform infrared spectroscopy. Compared to the conventional method, the proposed microwave-assisted method produced AuNPs having a small size of 22.07 ± 8.11 nm in a short synthesis time period. In excess $NaBH_4$, the as-prepared AuNPs demonstrated good catalytic activity for reducing 4-nitrophenol to 4-aminophenol. Furthermore, AuNPs demonstrated improved reusability after four cycles. The pseudo-first-order apparent rate constant was estimated to be 0.086 min^{-1} at 303 K. Both the catalytic mechanism and reaction path of reduction were proposed. Moreover, activation energy and thermodynamic parameters, including activation enthalpy and entropy, were examined.

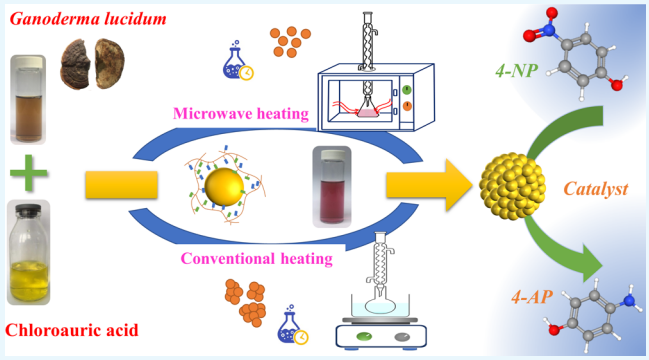

1. INTRODUCTION

4-Nitrophenol (4-NP) is one of the most poisonous and refractory contaminants generated from the production process of agriculture, pigments, and drugs;[1] it affects the blood, kidney, and central nervous system and has the ability to convert hemoglobin to methemoglobin, thus resulting in severe hypoxia.[2−4] 4-Aminophenol (4-AP) is less poisonous and is used as a precursor for producing analgesics and antipyretics.[5,6] Therefore, in both the environment and human life, the reduction of 4-NP to 4-AP using $NaBH_4$ as a reducing agent plays an important role. This reaction could occur only in the presence of a metal nanostructure as a catalyst.[7]

Among catalysts, gold nanoparticles (AuNPs) are one of the nanosized materials that have attracted considerable attention from researchers for the phenomenon of surface plasmon resonance (SPR) because of their unique optical properties.[8,9] AuNPs are synthesized using different physical and chemical methods.[10] The physical approach has many limitations, including high energy requirements, complex expensive instruments, and a low yield.[11] In terms of chemical synthesis, using a basic laboratory setup, the chemical approach is extremely cost-effective and has a high yield.[12] However, chemical methods use poisonous and volatile reactants, which are extremely dangerous and detrimental to both the environment and human health. Hence, researchers are interested in developing eco-friendly and inexpensive alternative protocols such as one-step synthesis of AuNPs utilizing some molecules as both the reducing and capping agent.[13,14] Consequently, for synthesizing AuNPs, the scientific community developed a novel green strategy. This method's protocol has been established using biobased reagents such as bacteria, fungi, marine algae, lichens, and plants.[15]

The idea of using plant extract of *Ganoderma lucidum* (*G. lucidum*) to generate nanostructures as a reducing and protecting agent has received the concern of scientists, such as silver nanoparticles[16] and reduced graphene oxide-magnetite nanocomposites.[17] *G. lucidum* is one of the biological agents and is commonly known as lingzhi in Chinese and reishi in Japanese; it has been used as a medicinal mushroom for the past centuries.[18] The extract is used to promote an extremely long life, a healthy immune system, and mental clarity because of its strong anti-inflammatory function. The *G. lucidum* composition contains multiple bioactive components such as

Received: September 12, 2021
Accepted: November 4, 2021
Published: November 17, 2021

polysaccharides, triterpenes, proteins, and a small amount of amino acids and vitamins,[19] which leads to it having medicinal properties, e.g., antiallergic,[20] anti-inflammatory,[21] antiviral,[22] and anticancer activities.[23] Therefore, as a reducing and preventing agglomeration agent, in the "green synthesis" process of AuNPs, the plant extract of *G. lucidum* was used.

Many studies reported that the rate of synthesizing metallic nanoparticles could be significantly higher using assistance techniques such as heat-treatment,[24] gamma irradiation,[25] ultrasonication,[26,27] hydrothermal,[28,29] and microwave irradiation.[30,31] Among these assistance techniques, microwave-assisted synthesis has been receiving attention as an inexpensive heating method because of its short reaction time, low cost, and high product output.[32] Thus, electromagnetic waves with irradiation ranging from 300 MHz to 300 GHz (corresponding to the wavelength varying from 1 m to 1 mm)[33] and microwave irradiation could directly interact with molecules and accelerate them. Thus, radiation energy dissipates to these molecules leading to an increase in the inner temperature of objects and homogeneous heating.[34] However, conventional heating methods tend to transfer heat from the surface to inner objects using convective thermal gradients; furthermore, the surface temperature of objects is higher than that of other parts, which leads to both a nonuniform heat distribution and a reduction in the productivity of the reaction.[35] Consequently, microwave-assisted synthesis seems a potential candidate for novel techniques that assist in the synthesis method of materials, particularly nanosized materials.[36]

In this study, the advancement of microwave-assisted green synthesis compared to conventional heating for preparing AuNPs was successfully demonstrated; furthermore, the optical and morphological properties, crystal phase, and size distribution of AuNPs were examined. Finally, the catalytic properties of AuNPs for reducing 4-NP were evaluated. Both activation energy and thermodynamic parameters were determined by reduction under different temperatures. This is the first study on the comprehensive microwave-assisted biosynthesis of AuNPs using *G. lucidum* extract and evaluation of their catalytic reduction of 4-nitrophenol.

2. RESULTS AND DISCUSSION

2.1. Characterization of the Obtained Materials.

Before the reaction, the mixture, including the *G. lucidum* aqueous extract and chloroauric acid, was yellow. After the reaction, the color of the mixture changed to dark purple. Because of SPR, this observation contributed to the confirmation of the formation of AuNPs. Moreover, a UV−vis spectrometer was used to examine the optical properties of MW-AuNPs and CH-AuNPs. Figure 1 shows the UV−vis spectra of these Au colloidal suspensions. Note that CH-AuNPs had the SPR peak at 537 nm; however, the SPR peak of MW-AuNPs shifted to a shorter wavelength at 525 nm. Moreover, this peak was sharper and at higher intensity than that of the CH-AuNP sample. Thus, with the help of microwave-assisted synthesis, additional particles with a uniform size distribution were obtained.

Figure 2 shows different magnified transmission electron microscopy (TEM) images and corresponding histograms of the particle size of CH-AuNPs and MW-AuNPs. Both samples are mostly spherical in shape; moreover, the size of CH-AuNPs (Figure 2a,b) is larger than that of CH-AuNPs (Figure 2d,e). Furthermore, particle size distribution histograms (Figure 2c,f)

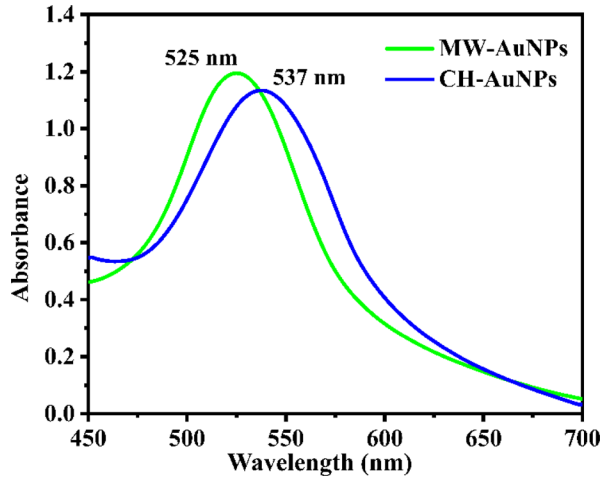

Figure 1. Comparison of UV−vis spectra of MW-AuNPs and CH-AuNPs.

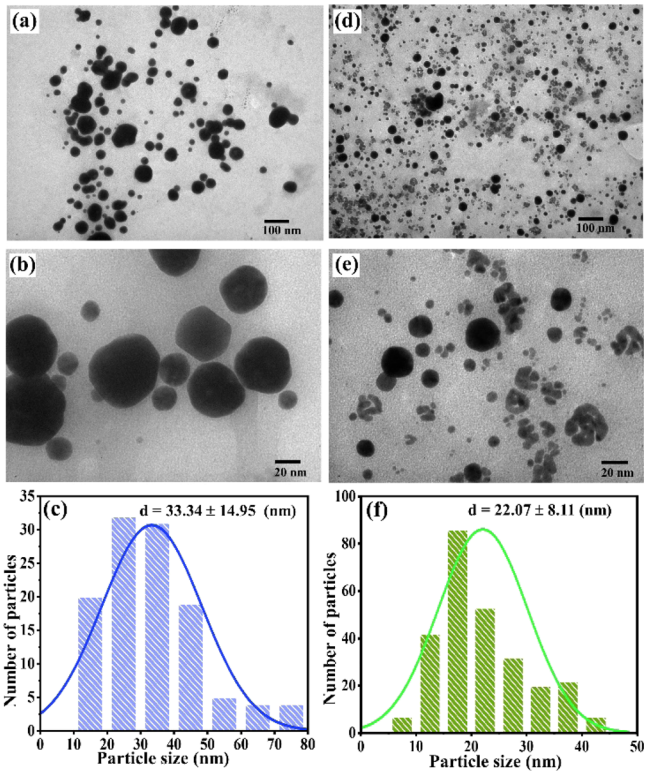

Figure 2. Different magnified TEM images and corresponding particle size distribution analysis of CH-AuNPs (a−c) and MW-AuNPs (d−f).

are obtained by measuring the size of particles from the corresponding TEM image (Figure 2a,d). CH-AuNPs have a wide range of size distribution at ∼33.34 ± 14.95 nm. However, the size distribution of MW-AuNPs was smaller with sizes at ∼22.07 ± 8.11 nm; moreover, these particles are quite uniform. As seen from the scanning electron microscopy (SEM) images in Figure 3, MW-AuNPs are more homogenously spherical and dispersed compared to the sample of CH-AuNPs.

Figure 4 shows the X-ray diffraction (XRD) patterns used to describe the crystal structure of the obtained nanoparticle samples. Au nanocrystals in the two samples demonstrated

https://doi.org/10.1021/acsomega.1c05033
ACS Omega 2021, 6, 32198−32207

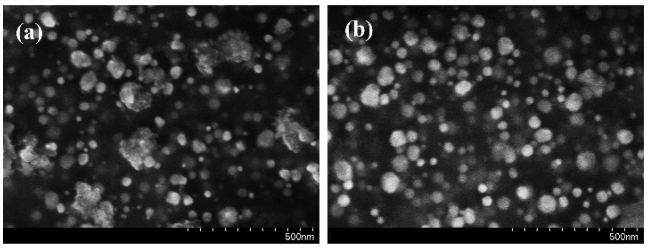

Figure 3. SEM images of CH-AuNPs (a) and MW-AuNPs (b).

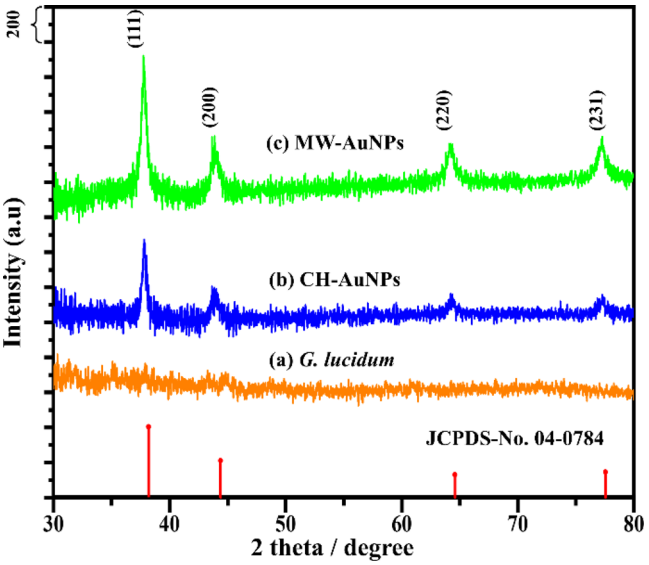

Figure 4. XRD patterns of *G. lucidum* (a), CH-AuNPs (b), and MW-AuNPs (c).

similar diffraction peaks to those from the standard XRD pattern of AuNPs (JCPDS No. 04−0784). There are four distinct peaks at 2θ = 37.7, 43.9, 64.2, and 77.2°, corresponding to (111), (200), (220), and (311) reflection planes of the fcc structure of metallic Au. Moreover, the crystallinity of MW-AuNPs was higher than that synthesized using conventional methods. The average crystallite size of AuNPs in MW-AuNPs and CH-AuNPs samples was determined using Scherrer's equation:

$$D = K\cdot\lambda/\beta\cdot\cos\theta \quad (1)$$

where D is the crystallite size (nm); K is the shape factor, usually taken as 0.9; λ is the wavelength of X-rays in nanometers ($\lambda_{\text{Cu K}\alpha}$ = 0.15405 nm); θ is the diffracted angle of the peak; and β is the full width at half maximum of the peak in radians. The results show that the average crystallite size of MW-AuNPs was less than that of CH-AuNPs (16.651 nm for MW-AuNPs and 18.656 nm for CH-AuNPs).

The XRD pattern of both samples has the same pattern as that of the TEM particle size. This observation could be explained by comparing the heating mechanism between these two methods: conventional heating and microwave heating (Figure 5).

Conventional heating comprises a combination of conductive and convective heat transfer, which leads to a slow increase in temperature. However, under microwave irradiation treatment, the temperature of the mixture significantly increased because of dipole rotation and ionic conduction.[37,38] Therefore, Au ions were homogenously heated with localized

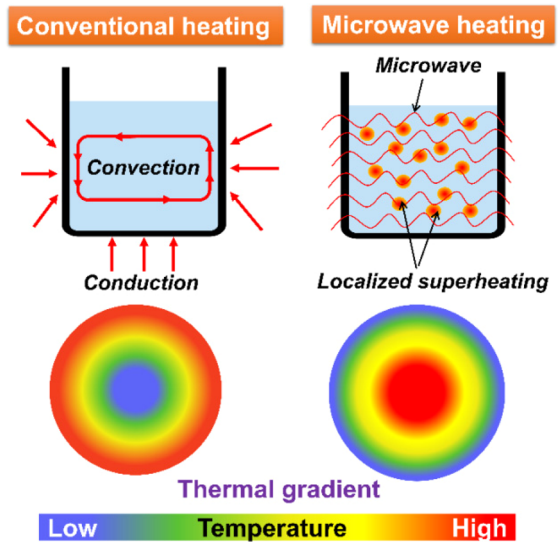

Figure 5. Comparison between conventional heating and microwave heating.

superheating, thus increasing the effective interactions between Au ions and functional groups such as hydroxyl and carbonyl in the aqueous extract of *G. lucidum*. Therefore, the reduction rate of the ion Au^{3+} to Au^0 significantly increased, which contributed to reduction in the reaction time and increase in the product yield. Moreover, microwave-assisted synthesis promptly promoted nucleation and simultaneously all nuclei grew. Therefore, with the help of microwave-assisted synthesis, MW-AuNPs have high crystallinity and produce smaller and uniform particles.

FTIR spectroscopy was performed to demonstrate functional groups capping on the surface of AuNPs. Figure 6 shows

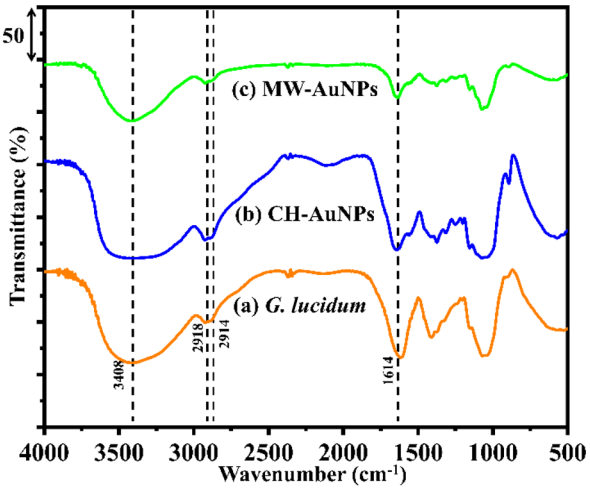

Figure 6. Fourier transform infrared (FTIR) spectra of GL extract (a), CH-AuNPs (b), and MW-AuNPs (c).

the FTIR spectra of GL extract, CH-AuNPs, and MW-AuNPs. In the spectrum of GL extract (Figure 6a), the absorption peak observed at 3408 cm^{-1} was attributed to the stretching vibration of hydroxyl groups. The peaks at 2914 and 1614 cm^{-1} were attributed to the methylene and carbonyl groups (−C═O), respectively.[39,40] Moreover, the peak appearing at ∼2918 cm^{-1} was attributed to the stretching of the C−N group. In terms of the spectra of CH-AuNPs and MW-AuNPs

https://doi.org/10.1021/acsomega.1c05033
ACS Omega 2021, 6, 32198−32207

(Figure 6b,c), there seems to be a similarity to the FTIR spectra of GL extract; these results confirm that there were certain functional groups in the surface of AuNPs in both CH-AuNP and MW-AuNP samples. However, the intensity of these peaks slightly decreased; this phenomenon could be explained by the hydrolysis of the GL extract in an alkaline environment (pH = 9) as well as the oxidation of hydroxyl groups and carbonyl groups, which involved reducing the ion Au^{3+} to Au^{0} during the synthesis of AuNPs in two different protocols.

The elemental compositions of MW-AuNPs were examined using the energy-dispersive X-ray spectroscopy (EDX) technique; furthermore, the EDX elemental mapping is shown in Figure 7. The EDX spectra show that the four

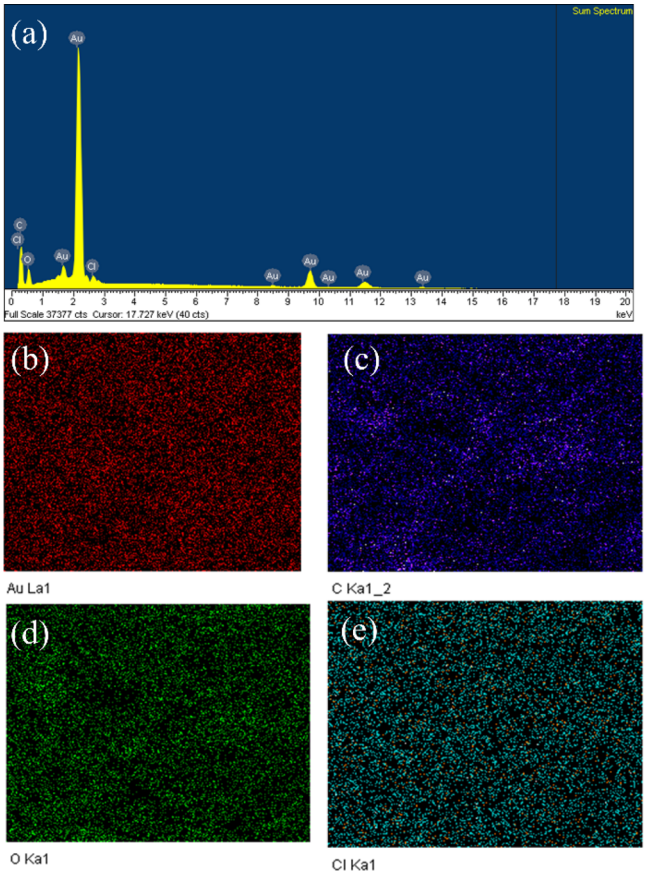

Figure 7. EDX spectrum of MW-AuNPs (a) and EDX elemental mapping of Au (b), C (c), O (d), and Cl (e).

main elements are Au, O, C, and Cl in the sample (Figure 7a); moreover, the amount of Au was the highest at 53.66% (Table 1). The elemental distribution was observed using the elemental mapping image (Figure 7b–e); these results show the well distribution of four elements, particularly Au in the nanostructure.

Table 1. Elemental Composition of MW-AuNPs Analyzed Using EDX

element	weight (%)	atom (%)
C	31.35	68.99
O	13.94	23.03
Cl	1.05	0.78
Au	53.66	7.20

2.2. Stability of the Suspension. The stability of the colloidal solution of the MW-AuNP sample was examined by obtaining the UV–vis spectra of samples stored at different times at room temperature; the result is shown in Figure 8a.

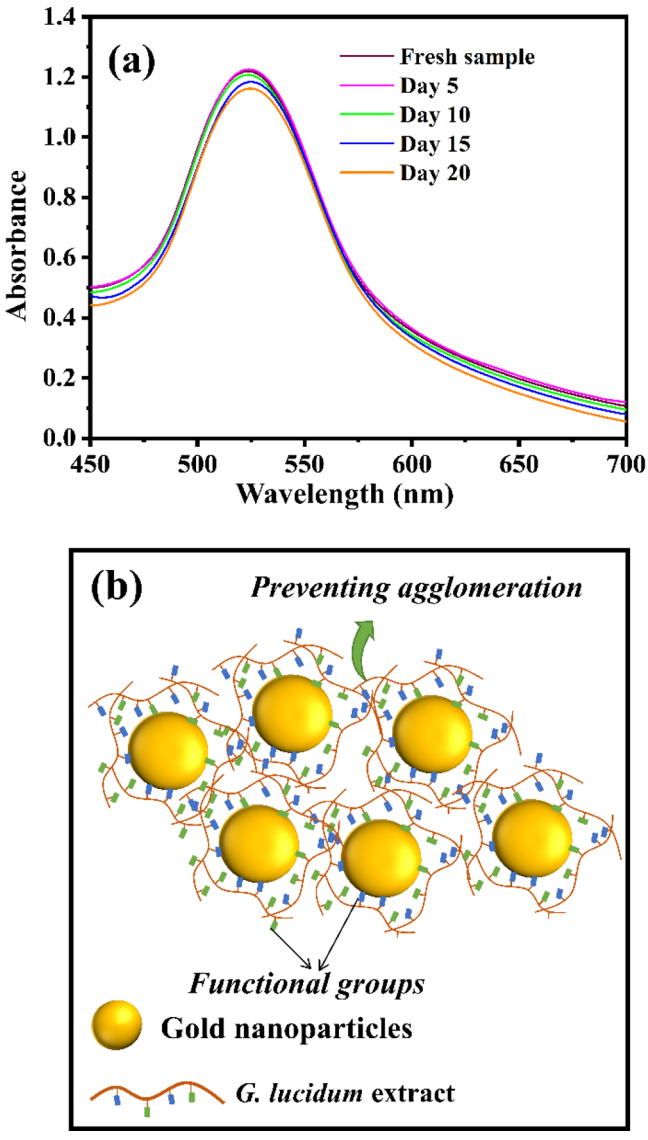

Figure 8. (a) UV–vis spectra of a colloidal solution of Au at different storage times and (b) scheme of preventing agglomeration between AuNPs.

The original sample demonstrated an SPR peak at an absorption of 525 nm. Although this absorption peak shifted to a longer wavelength (~530 nm) after 20 days with a slight decrease in the strength of absorption peaks, there was no visual agglomeration phenomenon of the colloidal solution of Au during the survey time. This indicates that the sample of MW-AuNPs is stable and could be stored for 3 weeks. This phenomenon could be explained by the fact that these functional groups of the GL extract have the ability to form a layer surrounding the surface of AuNPs (Figure 8b) to prevent agglomeration between AuNPs. Therefore, in the synthesis process of AuNPs, GL extract acts as both a reducing and stabilizing agent.

https://doi.org/10.1021/acsomega.1c05033
ACS Omega 2021, 6, 32198–32207

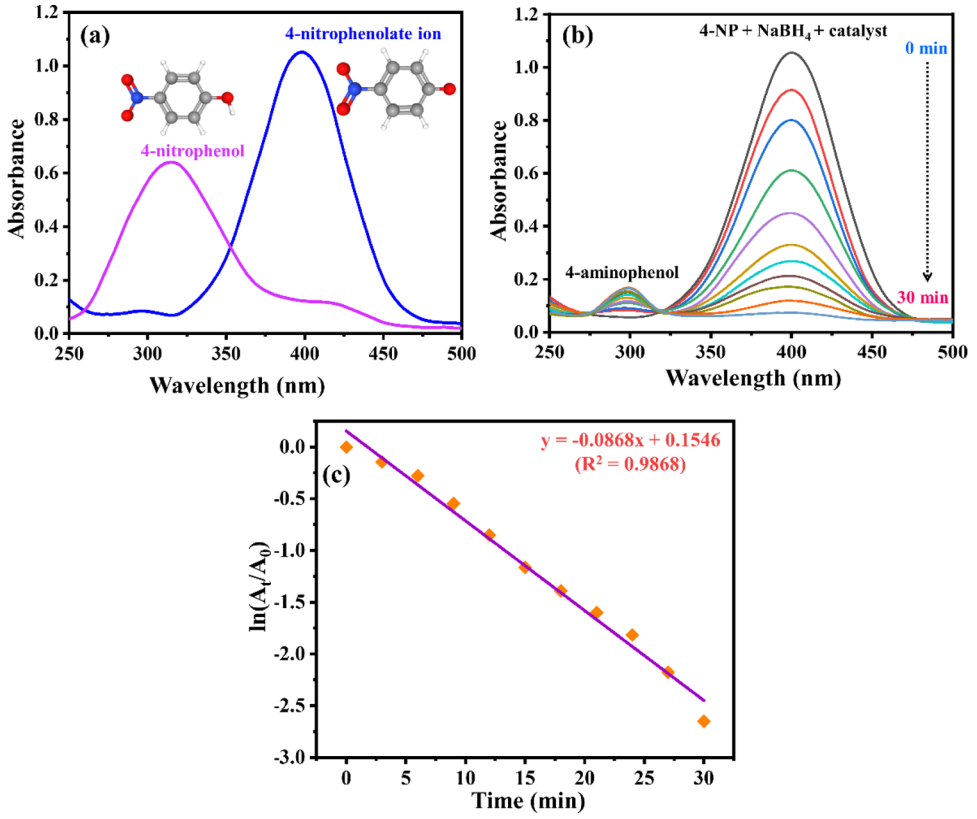

Figure 9. (a) UV−vis spectra of 4-NP before and after adding $NaBH_4$, (b) time-dependent UV−vis absorption spectra for reducing 4-NP using AuNPs as a catalyst, and (c) plot of $\ln(A_t/A_0)$ versus reaction time (reaction condition: $C_{4NP} : C_{NaBH_4} = 1 : 100$, 303 K, $m_{catalyst} = 1$ mg).

2.3. Catalytic Activity of MW-AuNPs for the Reduction of 4-NP. The reduction reaction of 4-NP to 4-AP with $NaBH_4$ was used to evaluate the catalytic properties of AuNPs. In an aqueous medium, the 4-NP solution demonstrates an absorption peak at 317 nm; then, while adding $NaBH_4$, the absorption peak shifted to a longer wavelength at 400 nm (Figure 9a) with change in color from light yellow to deep yellow, which was attributed to the generation of 4-nitrophenolate ions.[41] In the absence of the AuNP catalyst, the reduction of 4-NP cannot occur; furthermore, the color of the reaction mixture was immutable. In terms of the presence of a small amount of Au catalyst, by increasing the reaction time not only was there releasing of additional air bubbles but also the yellow color of 4-nitrophenolate became colorless. The time dependence of reduction of 4-NP was examined by monitoring the UV−vis spectra and is illustrated in Figure 9b. During the reaction time, the intensity of the peak at 400 nm related to 4-NP gradually decreased; however, the absorption peak of 4-AP at 300 nm increased and the reduction of 4-NP was complete after 30 min. As per the reaction condition, the $NaBH_4$ amount was considerably higher than the amount of 4-NP such that the concentration of 4-NP remains constant during the reduction reaction. Therefore, the reduction of 4-NP abides by the pseudo-first-order kinetics;[42] moreover, the apparent kinetic rate constant (k_{app}) was determined using eq 2:

$$\ln\left(\frac{A_t}{A_0}\right) = -k_{app}t \quad (2)$$

where A_0 and A_t are the absorbance of 4-NP (400 nm) at 0 and t min, respectively. The k_{app} value was calculated using the slope of the linear plot of $\ln(A_t/A_0)$ versus reaction time; the result is shown in Figure 9c. At 303 K, the apparent kinetic rate was 0.086 min^{-1} with $R^2 = 0.9868$.

In this study, the catalytic performance of AuNP synthesis obtained for the 4-NP reaction is compared with the previous results of Au nanosized materials and is presented in Table 2.

Table 2. Comparison of Studies on the Catalytic Reduction of 4-NP from Different Sources

biological source	particle size (nm)	k_{app} (min^{-1})	reference
Crinum latifolium leaf	17.6	0.206	43
Trichosporon montevideense	12−53	0.032	44
jujube	8−13	0.070	45
Lactuca indica leaf	14.5	0.078	46
Breynia rhamnoides	25	0.564	47
Ganoderma lucidum	22	0.086	*this work*

In this study, the k_{app} value was considerably less than the other material; these results could explain that the particle size of AuNPs synthesized by the extract of *G. lucidum* with the assistance of microwave-assisted spectroscopy was larger than that of other AuNP samples, as shown in Table 2; furthermore, the organic molecules covering the surface of MW-AuNPs could partially defend the active sites of nanoparticles, which affects the catalytic activity for reducing 4-NP.

For effective practical applications, the reusability of AuNPs as a catalyst plays an extremely important role. For the recycle process, AuNPs after each usage was centrifuged and washed three times with distilled water and then ethanol, followed by drying overnight for the next cycle of catalysis using the same reaction conditions. Figure 10 shows the effectiveness of

https://doi.org/10.1021/acsomega.1c05033
ACS Omega 2021, 6, 32198−32207

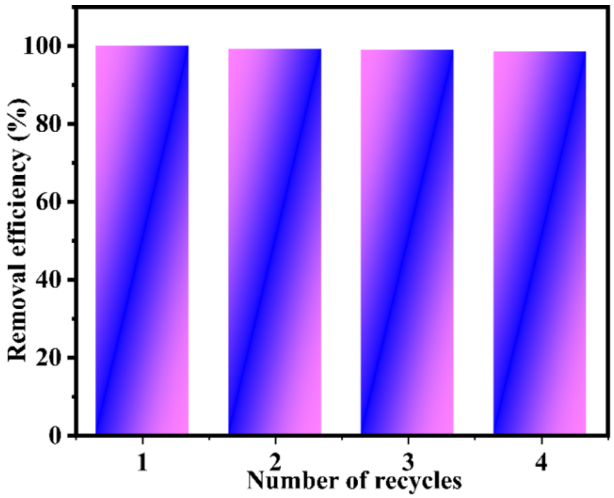

Figure 10. Reusability of the AuNP catalyst.

reducing AuNPs. There was a slight decrease in the value of the reduction efficiency after four cycles, which contributes to the fact that AuNPs are a potential catalyst for reducing 4-NP.

2.4. Proposed Mechanism for 4-NP Reduction by $NaBH_4$ in the Presence of Gold Nanoparticles. Figure 11 shows the reaction mechanism for the catalyst reduction of 4-NP in the presence of AuNPs and obeys the Langmuir–Hinshelwood model.[48−50] At the start of the process, excess BH_4^- ions from $NaBH_4$ are hydrolyzed in water to generate active hydrogen and then approach the AuNP catalyst and form the Au–H complex between the Au atom and active hydrogen.[51] In the subsequent step, the 4-NP molecules adsorb on the surface of AuNPs, and 4-NP, which was reduced by the active hydrogen of the Au hydride, complex to form 4-AP. Finally, 4-AP was desorbed from the surface of AuNPs, which can then recycle the surface for the next catalytic cycle.

2.5. Effect of Reaction Temperature. As various temperatures ranging from 303 to 333 K, the activation energy and thermodynamic parameters for reducing 4-NP by AuNPs were analyzed using the same protocol. The catalytic equipment was placed in a thermostat such that the temperature could be exactly adjusted. When increasing the reaction temperature, the movement of reactant molecules vigorously increase, leading to a more effective collision.[52] Therefore, the k_{app} values for reducing 4-NP increased with the increase in temperature; these results are observed in Figure 12a. To calculate the activation energy and thermodynamic parameters such as the activation enthalpy ($\Delta H^{\#}$), the activation entropy ($\Delta S^{\#}$) was calculated using the following equations:

Arrhenius equation:[53]

$$\ln k_{app} = \ln A - \frac{E_a}{RT} \tag{3}$$

Eyring equation:[54]

$$\ln \frac{k_{app}}{T} = \ln \frac{k_B}{h} + \frac{\Delta S^{\#}}{R} - \frac{\Delta H^{\#}}{RT} \tag{4}$$

Gibbs equation:

$$\Delta G^{\#} = \Delta H^{\#} - T \cdot \Delta S^{\#} \tag{5}$$

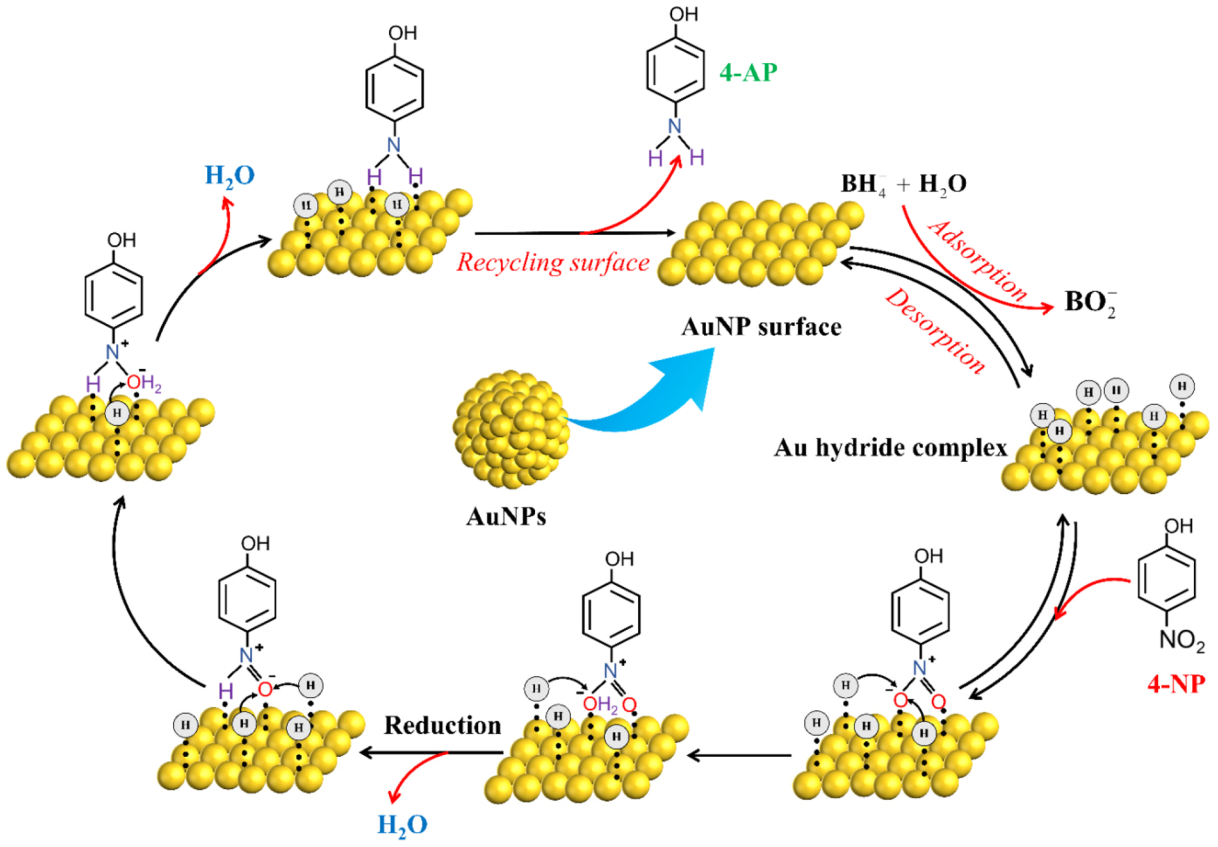

Figure 11. Schematic for the mechanism of reducing 4-NP in the presence of AuNPs as a catalyst.

https://doi.org/10.1021/acsomega.1c05033
ACS Omega 2021, 6, 32198−32207

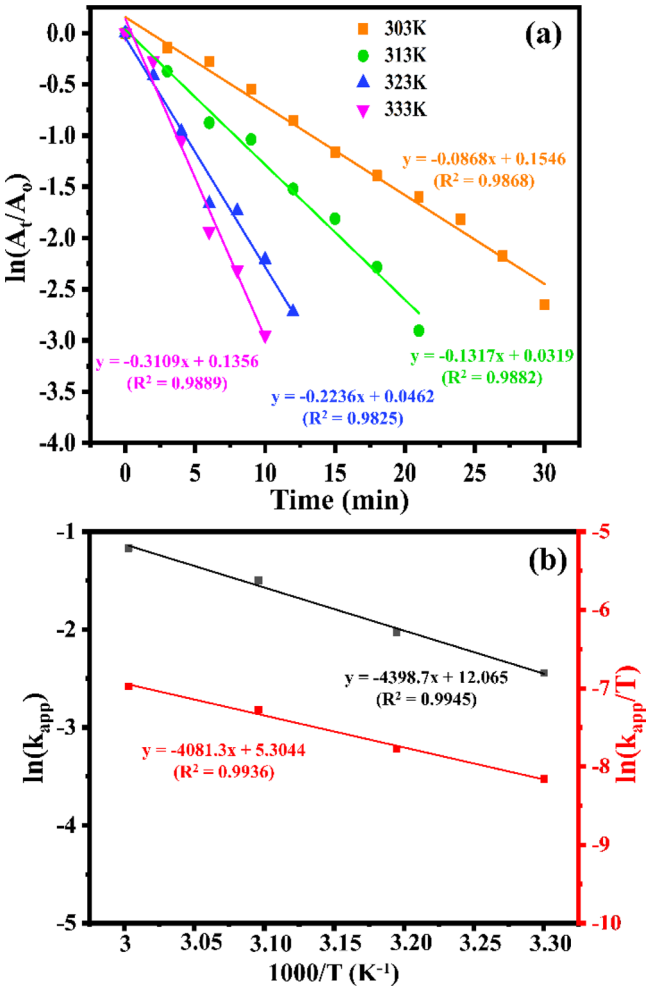

Figure 12. (a) Plot of $\ln(C/C_0)$ versus the reaction time at different reaction temperatures (303−333 K) and (b) plots of ln k_{app} (black line) and $\ln(k_{app}/T)$ (red line) versus $1/T$ (reaction condition: C_{4NP} : C_{NaBH_4} = 1 : 100, 303 K, and $m_{catalyst}$ = 1 mg).

where A is a constant, R is the gas constant (8.314 J·mol^{-1} K^{-1}), and k_{app} is the apparent rate constant at the investigated temperature T; T is the absolute temperature (in kelvin); E_a is the activation energy; k_B is the Boltzmann constant (1.381×10^{-23} J·K^{-1}), and h is Planck's constant (6.63×10^{-34} J·s).

E_a was defined using the slope of the linear plot of ln k_{app} versus $1/T$ (Figure 12b-black line) and obtained as 36.57 kJ·mol^{-1} with R^2 = 0.9945. However, $\Delta H^{\#}$ and $\Delta S^{\#}$ were obtained to be 33.931 kJ·mol^{-1} and −153.44 J·mol^{-1}·K^{-1}, respectively (Table 3), as per the slope and intercept of the linear plot of $\ln(k_{app}/T)$ versus $1/T$ (Figure 12b-red line). We then obtained a positive $\Delta H^{\#}$, which indicates that the formation of an activated complex between 4-NP molecules and AuNPs was endothermic. Furthermore, the negative value of $\Delta S^{\#}$ indicates that there was the formation of an activated complex between molecules of 4-NP and AuNPs.[55] Moreover, in the adsorption of 4-NP on the surface of AuNPs, the value of Gibbs free energy was positive, which indicates that the reaction required energy to convert reactants to products; furthermore, when the energy requirement was suitable, the reduction occurred.

Table 3. Result of Thermodynamic Parameters for Reducing 4-NP in the Presence of AuNPs as a Catalyst

temperature (K)	$\Delta H^{\#}$ (kJ mol^{-1})	$\Delta S^{\#}$ (J mol^{-1} K^{-1})	$\Delta G^{\#}$ (kJ mol^{-1})
303	33.931	−153.44	80.424
313			81.959
323			83.493
333			85.028

3. CONCLUSIONS

This study proposed that spherical AuNPs with an average size of 22 nm were synthesized using the *G. lucidum* extract with the help of microwave-assisted synthesis. The catalytic activity of reducing 4-NP was significantly higher in the presence of AuNPs with high stability and reusability for four catalytic cycles. The results of the thermodynamic studies of the reaction demonstrated that the activation energy value was 36.57 kJ·mol^{-1}. Furthermore, both activation enthalpy and activation entropy were reported to be 33.931 kJ·mol^{-1} and −153.44 J·mol^{-1}·K^{-1}, respectively. This study's outcome indicated that, as a reducing and preventing agglomeration agent, the plant extract of *G. lucidum* was used during the "green synthesis" process of AuNPs.

4. EXPERIMENTAL SECTION

4.1. Material. The fruit bodies of *G. lucidum* obtained from the buffer zone of Bach Ma National Park from Nam Dong District, Thua Thien Hue province, were dried and ground to powder.

$HAuCl_4 \cdot 3H_2O$ was purchased from Shanghai Zhanyun Chemical. $NaBH_4$, 4-NP, NH_4OH (25%), and ethanol (99%) were purchased from Sigma-Aldrich, USA. All the chemicals were used as-received without additional purification.

4.2. Method. *4.2.1. Preparation ofGanoderma lucidumExtract.* The hot aqueous extract of GL was prepared using the reflux method. A 5.0 g of fruit body powder of *G. lucidum* was added to distilled water (500 mL) and heated to 85 °C for 4 h with stirring. Then, the mixture was centrifuged at 4300 rpm for 20 min to remove the insoluble part. For biosynthesizing AuNPs, the resultant product was filtered and *G. lucidum* extract was stored in a refrigerator.

4.2.2. Biosynthesis of Gold Nanoparticles Using GL Extract. AuNPs were then synthesized as per two processes using the conventional heating method and with the assistance of microwave irradiation: CH-AuNPs and MW-AuNPs. In a typical process, 10 mL of 1 mM chloroauric acid was added to 90 mL of aqueous extract of GL; the pH of the mixture was then adjusted to 9 by adding ammonia solution (25%, v/v) dropwise. For the preparation process with the assistance of microwave irradiation, the reaction mixture was placed in a microwave oven to react for 10 min at 400 W. For the conventional method, the reaction mixture was heated with stirring at 120 rpm, 85 °C for 6 h. To isolate AuNPs, the suspension was precipitated using 95% ethanol (v/v), followed by centrifugation (4000 rpm, 20 min). The pellets obtained were then dried in an oven at 100 °C for 12 h and stored for studying both the physicochemical characteristics and catalytic activity.

4.3. Catalytic Activity of Gold Nanoparticles in the 4-NP Reduction Reaction. The catalytic activity of AuNPs in the 4-NP reduction reaction was performed in an aqueous solution at room temperature. For a typical catalytic reaction, 1

https://doi.org/10.1021/acsomega.1c05033
ACS Omega 2021, 6, 32198−32207

mL of 4-NP (1 mM) was mixed with 1 mL of $NaBH_4$ (0.1 M) and 8 mL of deionized water. In the subsequent step, 1 mg of the Au nanocatalyst was added and then the reaction was carried out at room temperature. Using UV−vis spectrometry, in the scanning range from 200 to 500 nm, the UV−vis spectra of the mixture were recorded with time to track the shifting absorption of the mixture.

4.4. Characterization. After synthesizing AuNPs, the optical properties of these samples were examined using a UV−Vis V-630 spectrophotometer. Both the crystal phase and purity of nanosized materials were examined using XRD (D8-Bruker, Germany) equipped with CuKα radiation (λ = 1.5406 Å). Both morphology and particle size distribution of the synthesized products were observed using a transmission electron microscope (JEOL-1010, Japan) integrated with a scanning electron microscope (JEOL JSM-6510, Japan). Moreover, the elemental and atomic weight composition of samples were examined by EDX. Furthermore, to identify the functional groups of multiple biomolecules in these samples, FTIR analysis was then performed using a R-Prestige-21 Shimadzu FTIR spectrophotometer using the KBr pellet method.

AUTHOR INFORMATION

Corresponding Authors

DongQuy Hoang − *Faculty of Materials Science and Technology, University of Science, Vietnam National University, Ho Chi Minh City 700000, Vietnam;* orcid.org/0000-0002-5494-6796; Email: htdquy@hcmus.edu.vn

Thai Hoa Tran − *Department of Chemistry, University of Sciences, Hue University, Hue City 530000, Vietnam;* Email: tthaihoa@hueuni.edu.vn

Authors

Vinh Phu Nguyen − *Department of Chemistry, University of Sciences, Hue University, Hue City 530000, Vietnam; Faculty of Basic Sciences, University of Medicine and Pharmacy, Hue University, Hue City 530000, Vietnam;* orcid.org/0000-0003-2389-3422

Hieu Le Trung − *Department of Chemistry, University of Sciences, Hue University, Hue City 530000, Vietnam*

Thu Huong Nguyen − *Department of Chemistry, University of Sciences, Hue University, Hue City 530000, Vietnam*

Complete contact information is available at: https://pubs.acs.org/10.1021/acsomega.1c05033

Author Contributions

V.P.N. did the conceptualization, methodology, investigation, validation, and writing of the original draft and acquired funding. H.L.T and T.H.N. contributed to investigation and analysis. Supervision, validation, and writing—review and editing were done by D.Q.H. and T.H.T.

Notes

The authors declare no competing financial interest.

ACKNOWLEDGMENTS

V.P.N. was funded by Vingroup Joint Stock Company and supported by the Domestic Master/PhD Scholarship Programme of Vingroup Innovation Foundation (VINIF), Vingroup Big Data Institute (VINBIGDATA), code VINIF.2020.ThS.38.

REFERENCES

(1) Zhang, J.; Chen, G.; Guay, D.; Chaker, M.; Ma, D. Highly Active PtAu Alloy Nanoparticle Catalysts for the Reduction of 4-Nitrophenol. *Nanoscale* **2014**, *6*, 2125−2130.

(2) Chang, G.; Luo, Y.; Lu, W.; Qin, X.; Asiri, A. M.; Al-Youbi, A. O.; Sun, X. Ag Nanoparticles Decorated Polyaniline Nanofibers: Synthesis, Characterization, and Applications toward Catalytic Reduction of 4-Nitrophenol and Electrochemical Detection of H_2O_2 and Glucose. *Catal. Sci. Technol.* **2012**, *2*, 800−806.

(3) Liang, Y.; Manioudakis, J.; Macairan, J.-R.; Askari, M. S.; Forgione, P.; Naccache, R. Facile Aqueous-Phase Synthesis of an Ultrasmall Bismuth Nanocatalyst for the Reduction of 4-Nitrophenol. *ACS Omega* **2019**, *4*, 14955−14961.

(4) Lu, W.; Ning, R.; Qin, X.; Zhang, Y.; Chang, G.; Liu, S.; Luo, Y.; Sun, X. Synthesis of Au Nanoparticles Decorated Graphene Oxide Nanosheets: Noncovalent Functionalization by TWEEN 20 in Situ Reduction of Aqueous Chloroaurate Ions for Hydrazine Detection and Catalytic Reduction of 4-Nitrophenol. *J. Hazard. Mater.* **2011**, *197*, 320−326.

(5) Zhang, Y.; Liu, S.; Lu, W.; Wang, L.; Tian, J.; Sun, X. In Situ Green Synthesis of Au Nanostructures on Graphene Oxide and Their Application for Catalytic Reduction of 4-Nitrophenol. *Catal. Sci. Technol.* **2011**, *1*, 1142−1144.

(6) Guo, M.; He, J.; Li, Y.; Ma, S.; Sun, X. One-Step Synthesis of Hollow Porous Gold Nanoparticles with Tunable Particle Size for the Reduction of 4-Nitrophenol. *J. Hazard. Mater.* **2016**, *310*, 89−97.

(7) Esumi, K.; Miyamoto, K.; Yoshimura, T. Comparison of PAMAM−Au and PPI−Au Nanocomposites and Their Catalytic Activity for Reduction of 4-Nitrophenol. *J. Colloid Interface Sci.* **2002**, *254*, 402−405.

(8) Iarossi, M.; Schiattarella, C.; Rea, I.; De Stefano, L.; Fittipaldi, R.; Vecchione, A.; Velotta, R.; Ventura, B. D. Colorimetric Immunosensor by Aggregation of Photochemically Functionalized Gold Nanoparticles. *ACS Omega* **2018**, *3*, 3805−3812.

(9) Wang, Z. Plasmon—Resonant Gold Nanoparticles for Cancer Optical Imaging. *Sci. China Phys. Mech. Astron.* **2013**, *56*, 506−513.

(10) Herizchi, R.; Abbasi, E.; Milani, M.; Akbarzadeh, A. Current Methods for Synthesis of Gold Nanoparticles. *Artif. Cells. Nanomed. Biotechnol.* **2016**, *44*, 596−602.

(11) Wang, Y.; Xia, Y. Bottom-up and Top-down Approaches to the Synthesis of Monodispersed Spherical Colloids of Low Melting-Point Metals. *Nano Lett.* **2004**, *4*, 2047−2050.

(12) Hussain, M. H.; Abu Bakar, N. F.; Mustapa, A. N.; Low, K.-F.; Othman, N. H.; Adam, F. Synthesis of Various Size Gold Nanoparticles by Chemical Reduction Method with Different Solvent Polarity. *Nanoscale Res. Lett.* **2020**, *15*, 140.

(13) Qin, X.; Li, Q.; Asiri, A. M.; Al-Youbi, A. O.; Sun, X. One-Pot Synthesis of Au Nanoparticles/Reduced Graphene Oxide Nanocomposites and Their Application for Electrochemical H_2O_2, Glucose, and Hydrazine Sensing. *Gold Bull.* **2014**, *47*, 3−8.

(14) Sun, X.; Jiang, X.; Dong, S.; Wang, E. One-step Synthesis and Size Control of Dendrimer-protected Gold Nanoparticles: A Heat-treatment-based Strategy. *Macromol. Rapid Commun.* **2003**, *24*, 1024−1028.

(15) Menon, S.; Rajeshkumar, S.; Venkat Kumar, S. A Review on Biogenic Synthesis of Gold Nanoparticles, Characterization, and Its Applications. *Res. Efficient Technol.* **2017**, *3*, 516−527.

(16) Nguyen, V. P.; Le Trung, H.; Nguyen, T. H.; Hoang, D.; Tran, T. H. Synthesis of Biogenic Silver Nanoparticles with Eco-Friendly Processes Using Ganoderma Lucidum Extract and Evaluation of Their Theranostic Applications. *J. Nanomater.* **2021**, *2021*, No. 6135920.

(17) Lee, X. J.; Lim, H. N.; Gowthaman, N. S. K.; Rahman, M. B. A.; Che Abdullah, C. A.; Muthoosamy, K. In-Situ Surface Functionalization of Superparamagnetic Reduced Graphene Oxide−Fe_3O_4 Nanocomposite via Ganoderma Lucidum Extract for Targeted Cancer Therapy Application. *Appl. Surf. Sci.* **2020**, *512*, No. 145738.

(18) Bishop, K. S.; Kao, C. H. J.; Xu, Y.; Glucina, M. P.; Paterson, R. R. M.; Ferguson, L. R. From 2000 Years of Ganoderma Lucidum to

Recent Developments in Nutraceuticals. *Phytochemistry* **2015**, *114*, 56−65.
(19) Boh, B.; Berovic, M.; Zhang, J.; Zhi-Bin, L. Ganoderma Lucidum and Its Pharmaceutically Active Compounds. *Biotechnol. Annu. Rev.* **2007**, *13*, 265−301.
(20) Tasaka, K.; Mio, M.; Izushi, K.; Akagi, M.; Makino, T. Anti-Allergic Constituents in the Culture Medium of Ganoderma Lucidum. (II) The Inhibitory Effect of Cyclooctasulfur on Histamine Release. *Agents Actions* **1988**, *23*, 157−160.
(21) Joseph, S.; Sabulal, B.; George, V.; Antony, K.; Janardhanan, K. Antitumor and Anti-Inflammatory Activities of Polysaccharides Isolated from Ganoderma Lucidum. *Acta Pharm.* **2011**, *61*, 335−342.
(22) Eo, S.-K. K.; Kim, Y.-S. S.; Lee, C.-K. K.; Han, S.-S. S. Antiviral Activities of Various Water and Methanol Soluble Substances Isolated from Ganoderma Lucidum. *J. Ethnopharmacol.* **1999**, *68*, 129−136.
(23) Kao, C.; Jesuthasan, A. C.; Bishop, K. S.; Glucina, M. P.; Ferguson, L. R. Anti-Cancer Activities of Ganoderma Lucidum: Active Ingredients and Pathways. *Funct. Food Health Dis.* **2013**, *3*, 48−65.
(24) Salavati-Niasari, M.; Davar, F.; Fereshteh, Z. Synthesis of Nickel and Nickel Oxide Nanoparticles via Heat-Treatment of Simple Octanoate Precursor. *J. Alloys Compd.* **2010**, *494*, 410−414.
(25) Misra, N.; Biswal, J.; Gupta, A.; Sainis, J. K.; Sabharwal, S. Gamma Radiation Induced Synthesis of Gold Nanoparticles in Aqueous Polyvinyl Pyrrolidone Solution and Its Application for Hydrogen Peroxide Estimation. *Radiat. Phys. Chem.* **2012**, *81*, 195−200.
(26) Fuentes-García, J. A.; Santoyo-Salzar, J.; Rangel-Cortes, E.; Goya, G. F.; Cardozo-Mata, V.; Pescador-Rojas, J. A. Effect of Ultrasonic Irradiation Power on Sonochemical Synthesis of Gold Nanoparticles. *Ultrason. Sonochem.* **2021**, *70*, No. 105274.
(27) Masjedi-Arani, M.; Salavati-Niasari, M. A Simple Sonochemical Approach for Synthesis and Characterization of Zn_2SiO_4 Nanostructures. *Ultrason. Sonochem.* **2016**, *29*, 226−235.
(28) Seku, K.; Gangapuram, B. R.; Pejjai, B.; Hussain, M.; Hussaini, S. S.; Golla, N.; Kadimpati, K. K. Eco-Friendly Synthesis of Gold Nanoparticles Using Carboxymethylated Gum Cochlospermum Gossypium (CMGK) and Their Catalytic and Antibacterial Applications. *Chem. Pap.* **2019**, *73*, 1695−1704.
(29) Ahmadian-Fard-Fini, S.; Salavati-Niasari, M.; Ghanbari, D. Hydrothermal Green Synthesis of Magnetic Fe_3O_4-Carbon Dots by Lemon and Grape Fruit Extracts and as a Photoluminescence Sensor for Detecting of E. Coli Bacteria. *Spectrochim. Acta A Mol. Biomol. Spectrosc.* **2018**, *203*, 481−493.
(30) Tsuji, M.; Hashimoto, M.; Nishizawa, Y.; Kubokawa, M.; Tsuji, T. Microwave-assisted Synthesis of Metallic Nanostructures in Solution. *Chem. − Eur. J.* **2005**, *11*, 440−452.
(31) Hosseinpour-Mashkani, S. M.; Mohandes, F.; Salavati-Niasari, M.; Venkateswara-Rao, K. Microwave-Assisted Synthesis and Photovoltaic Measurements of $CuInS_2$ Nanoparticles Prepared by Using Metal−Organic Precursors. *Mater. Res. Bull.* **2012**, *47*, 3148−3159.
(32) Horikoshi, S.; Serpone, N. *Microwaves in Nanoparticle Synthesis: Fundamentals and Applications*; John Wiley & Sons, 2013.
(33) Har-Kedar, I.; Bleehen, N. M. Experimental and Clinical Aspects of Hyperthermia Applied to the Treatment of Cancer with Special Reference to the Role of Ultrasonic and Microwave Heating. *Adv. Radiat. Biol.* **1976**, *6*, 229−266.
(34) Palma, V.; Barba, D.; Cortese, M.; Martino, M.; Renda, S.; Meloni, E. Microwaves and Heterogeneous Catalysis: A Review on Selected Catalytic Processes. *Catalysts* **2020**, *10*, 246.
(35) Dahal, N.; García, S.; Zhou, J.; Humphrey, S. M. Beneficial Effects of Microwave-Assisted Heating versus Conventional Heating in Noble Metal Nanoparticle Synthesis. *ACS Nano* **2012**, *6*, 9433−9446.
(36) Yadav, A. R.; Mohite, S. K. A Brief Review: Microwave Chemistry and Its Applications. *Res. J. Pharm. Dos. Forms Technol.* **2020**, *12*, 191−197.
(37) Yoshikawa, N. Mechanism of Microwave Heating of Matter. In *RF power semiconductor generator application in heating and energy utilization*; Springer: Singapore, 2020, pp. 71−89.
(38) Dutta, D. P. Microwave-Assisted Synthesis of Inorganic Nanomaterials. In *Hanbook on Synthesis Stratergies for Advanced Materials*; Springer, 2021; pp. 79−107.
(39) Ibrahim, M.; Alaam, M.; el-Haes, H.; Jalbout, A. F.; Leon, A. Analysis of the Structure and Vibrational Spectra of Glucose and Fructose. *Eclet. Quím.* **2006**, *31*, 15−21.
(40) Wang, J.; Zhang, L. Structure and Chain Conformation of Five Water-Soluble Derivatives of a β-D-Glucan Isolated from Ganoderma Lucidum. *Carbohydr. Res.* **2009**, *344*, 105−112.
(41) Wu, G.; Liang, X.; Zhang, L.; Tang, Z.; Al-Mamun, M.; Zhao, H.; Su, X. Fabrication of Highly Stable Metal Oxide Hollow Nanospheres and Their Catalytic Activity toward 4-Nitrophenol Reduction. *ACS Appl. Mater. Interfaces* **2017**, *9*, 18207−18214.
(42) Chiu, C.-Y.; Chung, P.-J.; Lao, K.-U.; Liao, C.-W.; Huang, M. H. Facet-Dependent Catalytic Activity of Gold Nanocubes, Octahedra, and Rhombic Dodecahedra toward 4-Nitroaniline Reduction. *J. Phys. Chem. C* **2012**, *116*, 23757−23763.
(43) Vo, T.-T.; Nguyen, T. T.-N.; Huynh, T. T.-T.; Vo, T. T.-T.; Nguyen, T. T.-N.; Nguyen, D.-T.; Dang, V.-S.; Dang, C.-H.; Nguyen, T.-D. Biosynthesis of Silver and Gold Nanoparticles Using Aqueous Extract from Crinum Latifolium Leaf and Their Applications Forward Antibacterial Effect and Wastewater Treatment. *J. Nanomater.* **2019**, *2019*, 1.
(44) Shen, W.; Qu, Y.; Pei, X.; Zhang, X.; Ma, Q.; Zhang, Z.; Li, S.; Zhou, J. Green Synthesis of Gold Nanoparticles by a Newly Isolated Strain Trichosporon Montevideense for Catalytic Hydrogenation of Nitroaromatics. *Biotechnol. Lett.* **2016**, *38*, 1503−1508.
(45) Cui, Y.; Guo, X.; Lai, X.; Sun, H.; Liang, B.; Hou, W.; Liu, X.; Wang, L. Green Synthesis of Jujube-Polysaccharide-Stabilized Gold Nanoparticles for Reduction of 4-Nitrophenol. *ChemistrySelect* **2019**, *4*, 11483−11487.
(46) Vo, T.-T.; Dang, C.-H.; Doan, V.-D.; Dang, V.-S.; Nguyen, T.-D. Biogenic Synthesis of Silver and Gold Nanoparticles from Lactuca Indica Leaf Extract and Their Application in Catalytic Degradation of Toxic Compounds. *J. Inorg. Organomet. Polym. Mater.* **2020**, *30*, 388−399.
(47) Gangula, A.; Podila, R.; M, R.; Karanam, L.; Janardhana, C.; Rao, A. M. Catalytic Reduction of 4-Nitrophenol Using Biogenic Gold and Silver Nanoparticles Derived from Breynia Rhamnoides. *Langmuir* **2011**, *27*, 15268−15274.
(48) Wunder, S.; Polzer, F.; Lu, Y.; Mei, Y.; Ballauff, M. Kinetic Analysis of Catalytic Reduction of 4-Nitrophenol by Metallic Nanoparticles Immobilized in Spherical Polyelectrolyte Brushes. *J. Phys. Chem. C* **2010**, *114*, 8814−8820.
(49) Naseer, F.; Ajmal, M.; Bibi, F.; Farooqi, Z. H.; Siddiq, M. Copper and Cobalt Nanoparticles Containing Poly (Acrylic Acid-co-acrylamide) Hydrogel Composites for Rapid Reduction of 4-nitrophenol and Fast Removal of Malachite Green from Aqueous Medium. *Polym. Compos.* **2018**, *39*, 3187−3198.
(50) Noh, J.-H.; Meijboom, R. Catalytic Evaluation of Dendrimer-Templated Pd Nanoparticles in the Reduction of 4-Nitrophenol Using Langmuir−Hinshelwood Kinetics. *Appl. Surf. Sci.* **2014**, *320*, 400−413.
(51) Zhang, Y.; Cui, Z.; Li, L.; Guo, L.; Yang, S. Two-Dimensional Structure Au Nanosheets Are Super Active for the Catalytic Reduction of 4-Nitrophenol. *Phys. Chem. Chem. Phys.* **2015**, *17*, 14656−14661.
(52) Nemanashi, M.; Meijboom, R. Synthesis and Characterization of Cu, Ag and Au Dendrimer-Encapsulated Nanoparticles and Their Application in the Reduction of 4-Nitrophenol to 4-Aminophenol. *J. Colloid Interface Sci.* **2013**, *389*, 260−267.
(53) Saha, S.; Pal, A.; Kundu, S.; Basu, S.; Pal, T. Photochemical Green Synthesis of Calcium-Alginate-Stabilized Ag and Au Nanoparticles and Their Catalytic Application to 4-Nitrophenol Reduction. *Langmuir* **2010**, *26*, 2885−2893.

https://doi.org/10.1021/acsomega.1c05033
ACS Omega 2021, 6, 32198−32207

(54) Thawarkar, S. R.; Khupse, N. D.; Kumar, A. Kinetic Profile and Catalytic Activity of Transition Metal-based Ionic Liquids for Reduction of Nitroarenes via in Situ Formation of Nanoparticles. *ChemistrySelect* **2017**, *2*, 6833−6843.
(55) Iben Ayad, A.; Luart, D.; Ould Dris, A.; Guénin, E. Kinetic Analysis of 4-Nitrophenol Reduction by "Water-Soluble" Palladium Nanoparticles. *Nanomaterials* **2020**, *10*, 1169.

https://doi.org/10.1021/acsomega.1c05033
ACS Omega 2021, 6, 32198−32207